BILINGUAL PUBLISHING GROUP

Journal of Building Material Science

https://journals.bilpubgroup.com/index.php/jbms

ARTICLE

Local Interface Displacement and Global Response of Two-Layer Reinforced Concrete Slabs under Concentrated Loading

T. Q. K. Lam [*] ***, Chi-Hieu Dang***

Faculty of Civil Engineering, Mien Tay Construction University, Vinh Long 85119, Vietnam; dchieuchxd03@mtu.edu.vn

ABSTRACT

Two-layer reinforced concrete (RC) slabs are commonly used in staged construction, repair, and strengthening, yet the relationship between local interface displacement and global slab response remains insufficiently understood. This study investigated six slabs measuring 1,200 × 1,600 × 120 mm under monotonic concentrated loading. The series comprised one monolithic reference slab and five two-layer slabs with different layer arrangements and reinforcement configurations. The second layer was cast 14 days after the first layer using cement slurry at the interface and without mechanical connectors. Load, deflection, average surface strain, crack development, and local relative displacement in the long-span and short-span directions were recorded. The first visible cracks were observed at the 38 kN loading stage. The highest recorded test load was 50 kN for S1 and S2 and 63 kN for S3–S6. S4 showed the largest long-span interface displacement of 6.88 mm, whereas S3 showed the largest short-span value of 3.36 mm; S5 and S6 recorded smaller short-span values of 0.69 and 0.50 mm, respectively. The results show that global stiffness and local interface compatibility may evolve differently after cracking. These findings provide experimental evidence of partial composite action in two-layer slabs and highlight the importance of combining local interface measurements in both principal directions with global load–deflection and crack observations when assessing staged-cast or repaired reinforced concrete slabs.

Keywords: Local Interface Displacement; Two-Layer Reinforced Concrete Slab; Concentrated Loading; Global Response; Partial Composite Action

*CORRESPONDING AUTHOR:

T. Q. K. Lam, Faculty of Civil Engineering, Mien Tay Construction University, Vinh Long 85119, Vietnam; Email: Lamkhai@mtu.edu.vn

ARTICLE INFO

Received: 17 July 2026 | Revised: 28 July 2026 | Accepted: 12 August 2026 | Published Online: 20 October 2026
DOI: https://doi.org/10.30564/jbms.v8i4.117235

CITATION

Lam, T.Q.K., Dang, C.-H., 2026. Local Interface Displacement and Global Response of Two-Layer Reinforced Concrete Slabs under Concentrated Loading. Journal of Building Material Science. 8(4): 38–56. DOI: https://doi.org/10.30564/jbms.v8i4.117235

COPYRIGHT

Copyright © 2026 by the author(s). Published by Bilingual Publishing Group. This is an open access article under the Creative Commons Attribution-NonCommercial 4.0 International (CC BY-NC 4.0) License (https://creativecommons.org/licenses/by-nc/4.0/).

1. Introduction

Concrete members are often cast in more than one stage in repair works, strengthening with toppings, precast-cast-in-place construction, bridge deck overlays and staged construction of building slabs. In these cases, the plane between the hardened substrate and the newly placed concrete is not only a construction joint; it is a mechanical interface that must transfer shear while the member bends and cracks. The final response of the slab depends on concrete strength and flexural reinforcement, but also on whether this interface can keep the two layers working together. When the interface stiffness is insufficient, local relative displacement may develop between the layers, composite action may become partial, and the slab may exhibit increased deflection, strain redistribution, localized cracking, and reduced serviceability or durability.

The behavior of concrete-to-concrete interfaces has been widely investigated at the material and local-interface levels. Beushausen et al.[1] studied the influence of substrate moisture preparation on concrete overlays and showed that surface moisture condition can significantly affect bond strength and the microstructure of the overlay transition zone. Bentz et al.[2] further demonstrated that the measured bond performance depends on both substrate surface condition and test method, especially when comparing slant shear and pull-off tests. These studies indicate that the concrete-to-concrete interface should not be treated as a perfect contact plane, but as a transition zone whose behavior depends on casting condition, surface preparation and local stress state.

At the mechanical level, interface shear transfer is generally governed by the combined effects of adhesion, cohesion, aggregate interlock, friction under normal compression and, when present, reinforcement crossing the interface. Cavaco and Camara[3] showed that a concrete-to-concrete interface subjected to combined shear and bending behaves differently from an interface under direct shear alone. Cavaco et al.[4] also reported that interface detailing can influence ductility and failure mode. These findings are important because structural members such as slabs and beams are rarely subjected to pure interface shear; instead, interface shear develops together with bending deformation, cracking and strain redistribution.

Experimental studies using push-off, direct shear and composite specimens have clarified the influence of several interface parameters. Jiang et al.[5] investigated interface shear behavior between high-strength precast girders and lightweight cast-in-place slabs. Fang et al.[6] studied horizontal shear behavior in normal-weight and lightweight concrete composite T-beams. Liu et al.[7] evaluated design provisions for shear transfer between concretes cast at different times, while Davaadorj et al.[8] compiled a large experimental database to assess available interface shear strength models. Other studies[9–13] have examined the effects of surface treatment, normal stress, reinforcement ratio, corrosion, cyclic loading and concrete type on interface shear resistance[14–17]. These studies are valuable for identifying the main parameters controlling interface shear strength. However, most of them were based on local-interface specimens or simplified stress states, and therefore provide limited information on the development of local interface displacement in slab members under concentrated loading.

Composite beam studies provide a closer structural analogy because they consider the interaction between the interface and the global member response. Rueda-García et al.[18] investigated the shear strength of monolithic and composite concrete beams without web reinforcement, while Rueda-García et al.[19] studied precast concrete T-beams with a top cast-in-place slab. These studies confirmed that the interface can influence global shear resistance and structural performance. Nevertheless, beams are primarily one-dimensional members, whereas slabs subjected to concentrated loading develop two-way bending, multidirectional cracking and more complex slip redistribution. Accordingly, the interface behavior observed in composite beams cannot be directly extended to two-way slab systems.

Recent studies involving ultra-high-performance concrete, engineered cementitious composites, surface treatments, and other repair materials have further demonstrated that interface response depends on the properties of both the substrate and the newly placed material[16,20–22]. Broader studies on fibre-reinforced concrete, reinforcement detailing, and flexural performance also indicate that material condition and reinforcement configuration influence cracking and post-cracking deformation[23–25]. However, these investigations did not directly measure local relative displacement between the concrete layers of two-way reinforced concrete slabs under concentrated loading.

Design standards provide useful strength-based pro-

visions for checking interface shear resistance. EN 1992-1-1[26], ACI 318-19[27], AASHTO LRFD[28] and TCVN 5574:2018[29] include different approaches for estimating shear transfer across concrete-to-concrete interfaces or contact joints. These models are useful for strength verification, but they do not directly predict local interface displacement, post-cracking interface stiffness, directional displacement development, or the coupling between local interface response and global slab deformation. As a result, experimental load–interface displacement and load–deflection data remain necessary for evaluating the composite response of two-layer reinforced concrete slabs.

The literature still leaves several points unresolved for the type of member studied here. Most interface shear data come from push-off, direct shear, slant shear or beam specimens, while a two-way slab under a concentrated load develops bending, transverse shear and cracking in more than one direction. Code equations are also strength-oriented; they check whether interface resistance is sufficient, but they do not describe the measured load–interface displacement response after cracking. In addition, the position of the casting interface within the 120 mm slab thickness may change strain compatibility and shear-transfer demand, but this effect is not well documented for two-layer slabs. The influence of ordinary flexural reinforcement is also uncertain, because bars that do not cross the interface may still influence local interface displacement indirectly through changes in cracking and deflection. For these reasons, local relative interface displacement needed to be measured in both the long-span and short-span directions and interpreted together with the global slab response.

Accordingly, the study addressed three research questions. First, how are changes in layer arrangement and interface position associated with the local relative displacement measured in the long-span and short-span directions? Second, how is the measured interface response associated with changes in reinforcement configuration and reinforcement amount? Third, can the highest recorded load and global deflection alone adequately represent the degree of composite action in a two-layer slab?

It was hypothesized that changes in layer arrangement and interface position would be associated with different directional displacement responses after cracking; that changes in reinforcement configuration and reinforcement amount would modify the post-cracking response; and that global load and deflection measurements alone would not fully describe local compatibility between the two concrete layers.

To address these questions, six reinforced concrete slabs were tested under monotonic concentrated loading, including one monolithic reference slab and five slabs cast in two layers. The principal comparison factors were the layer arrangement, the position of the casting interface, and the reinforcement configuration and amount. Local relative interface displacement was measured in two orthogonal directions and interpreted together with vertical deflection, surface strain, visible crack development, and the highest recorded test load. The main contribution of the study is the simultaneous comparison of local interface displacement and global response in two-way layered slabs rather than in isolated interface or one-dimensional beam specimens.

2. Materials and Methods

2.1. Interface Transfer Mechanisms and Design-Code Context

2.1.1. General Mechanism of Interface Shear Transfer

The shear transfer mechanism at a concrete-to-concrete interface is governed by several interacting components, including adhesion, cohesion, aggregate interlock, friction and, when present, reinforcement or mechanical connectors crossing the interface. At the early loading stage, adhesion and cohesion may provide an initial bond between the hardened concrete substrate and the newly cast concrete layer. As load increases and cracking develops, the contribution of the initial bond decreases, and the interface resistance becomes more dependent on aggregate interlock, friction and any available clamping action.

For members cast in two stages, the interface must transfer horizontal shear so that the two concrete layers can act compositely. In general form, the design requirement may be written as Equation (1):

$$V_{Ed} \leq V_R \tag{1}$$

where V_{Ed} is the design interface force demand and V_R is the corresponding interface shear resistance.

Current design standards estimate the interface shear resistance in stress or force form using parameters such as

interface roughness, concrete strength, normal stress, friction coefficient and reinforcement crossing the shear plane. These parameters are useful for strength verification, but they do not directly describe the complete load–slip response. Accordingly, the design-code models are used in this study only as theoretical references for interpreting interface transfer mechanisms rather than as direct predictors of the measured local relative displacement.

2.1.2. Load–Displacement Response and Partial Composite Action

The response of a two-layer slab may be interpreted through the relationship between applied load and local relative interface displacement. Before visible cracking, initial adhesion and interface contact generally provide relatively high stiffness, allowing the two concrete layers to deform with limited relative movement. After cracking, degradation of the initial bond, changes in interface contact, and redistribution of flexural strains may increase the measured displacement between the layers.

This response represents partial composite action, in which both concrete layers continue to contribute to the structural response but no longer maintain complete deformation compatibility. Consequently, global load or deflection measurements may not fully represent the local condition of the casting interface. In the present study, load–interface displacement curves are therefore interpreted together with deflection, strain, and crack observations.

2.1.3. Summary of Design-Code Approaches

Several design standards provide provisions for shear transfer across concrete-to-concrete interfaces. EN 1992-1-1 [26] considers interface shear resistance as the sum of cohesion, friction due to normal stress, and reinforcement contribution. The design interface shear stress is checked against the design interface shear resistance using Equation (2):

$$\upsilon_{Edi} \leq \upsilon_{Rdi} \tag{2}$$

where υ_{Edi} is the design interface shear stress and υ_{Rdi} is the design interface shear resistance.

The design interface resistance is expressed by Equation (3):

$$\upsilon_{Rdi} = cf_{ctd} + \mu\sigma_n + \rho f_{yd}(\mu \sin\alpha + \cos\alpha) \leq 0.5\upsilon f_{cd} \tag{3}$$

where c and μ depend on interface roughness, f_{ctd} is the design tensile strength of concrete, σ_n is the normal stress across the interface, ρ is the reinforcement ratio crossing the interface, f_{yd} is the design yield strength of reinforcement, α is the angle of the reinforcement crossing the interface, υ is the strength reduction factor and f_{cd} is the design compressive strength of concrete.

ACI 318-19 [27] uses the shear-friction concept. For reinforcement crossing the shear plane, the nominal shear strength may be expressed as Equation (4):

$$V_n = \mu A_{vf} f_y \tag{4}$$

where A_{vf} is the area of shear-friction reinforcement, f_y is the yield strength of reinforcement and μ is the coefficient of friction. ACI also imposes upper limits on the nominal shear strength depending on concrete strength, interface area and surface condition.

AASHTO LRFD [28] expresses the nominal interface shear resistance as the sum of cohesion, friction, and clamping contributions Equation (5):

$$V_{ni} = cA_{cv} + \mu(A_{vf} f_y + P_c) \tag{5}$$

where c is the cohesion coefficient, A_{cv} is the concrete area engaged in interface shear transfer, μ is the friction coefficient, A_{vf} is the area of reinforcement crossing the interface, f_y is its yield strength, and P_c is the permanent net compressive force normal to the interface.

TCVN 5574:2018 [29] provides provisions for contact joints in concrete and reinforced concrete members. For an unreinforced contact joint, the sliding resistance may be expressed as Equation (6):

$$Q_j \leq \gamma_{b,sh,j} R_{bt} A_{b,j} \tag{6}$$

where Q_j is the sliding force at the joint, R_{bt} is the design tensile strength of concrete, $A_{b,j}$ is the contact area and $\gamma_{b,sh,j}$ is a coefficient related to joint preparation. For reinforced contact joints, the resistance may be increased by the reinforcement contribution.

The above provisions are strength-based and were not applied quantitatively to the tested specimens. A specimen-specific code verification was not performed because quantitative interface roughness, normal stress distribution, and other required input parameters were not measured in the experimental program. Moreover, these provisions do not directly predict the local load–displacement response recorded

by the dial gauges. The equations are therefore included only to provide a mechanical and design-code context for the experimental observations.

2.2. Experimental Program

2.2.1. Specimen Design

The experimental program consisted of six reinforced concrete slab specimens, designated S1 to S6. All specimens had the same plan dimensions of 1,200 mm × 1,600 mm and a total thickness of 120 mm. Specimen S1 was cast monolithically and was used as the reference slab. Specimens S2 to S6 were cast in two concrete layers to investigate local relative interface displacement and global slab response under concentrated loading.

The specimen design was developed to compare two main groups of variables: layer arrangement and interface position, and reinforcement configuration and amount. Specimens S2, S3, and S4 had the same reinforcement arrangement but different layer thicknesses. Because B15 concrete was used in the first layer and B20 concrete in the second layer, this comparison represented the combined changes in layer arrangement, interface position, and through-depth concrete-strength distribution. Specimens S5 and S6 were used to compare different reinforcement configurations while maintaining the 70 + 50 mm layer arrangement. S5 used Ø6 bars at 150 mm spacing, whereas S6 used Ø8 bars at 200 mm spacing. The corresponding reinforcement areas were approximately 188 mm^2/m for S5 and 251 mm^2/m for S6, compared with approximately 141 mm^2/m for the Ø6@200 mm configuration used in S2. Therefore, the comparisons represent the combined effects of reinforcement spacing, bar diameter, and reinforcement amount; these parameters were not isolated independently. The specimen details are summarized in **Table 1**.

In **Table 1**, Ø6@200 mm denotes 6 mm diameter reinforcing bars spaced at 200 mm, and Ø8@200 mm denotes 8 mm diameter reinforcing bars spaced at 200 mm.

Specimens S2, S3, and S4 were used to compare different layer arrangements and interface positions. In these specimens, the reinforcement arrangement was kept constant as Ø6@200 mm, while the relative thicknesses of the two concrete layers were varied. Specimen S2 consisted of a 70 mm first layer and a 50 mm second layer, S3 consisted of two equal 60 mm layers, and S4 consisted of a 50 mm first layer and a 70 mm second layer.

The geometric configuration and interface location of the specimens are illustrated in **Figure 1**.

Table 1. Specimen details and main experimental variables.

Specimen	Casting Type	Layer Thickness, mm	Reinforcement	Main Variable
S1	Monolithic	120	Ø6@200	Reference slab
S2	Two-layer	70 + 50	Ø6@200	Reference two-layer slab
S3	Two-layer	60 + 60	Ø6@200	60 + 60 mm layer arrangement
S4	Two-layer	50 + 70	Ø6@200	50 + 70 mm layer arrangement
S5	Two-layer	70 + 50	Ø6@150	Reduced spacing and increased steel area
S6	Two-layer	70 + 50	Ø8@200	Larger diameter and increased steel area

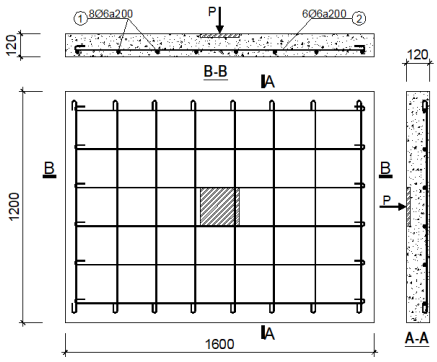

(**a**) S1 Specimen.

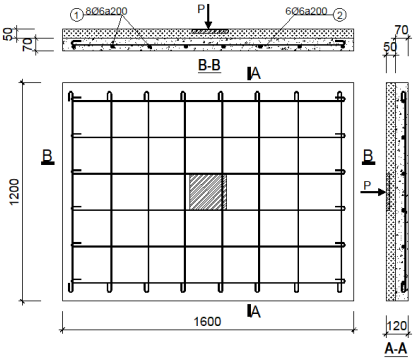

(**b**) S2 Specimen.

Figure 1. *Cont.*

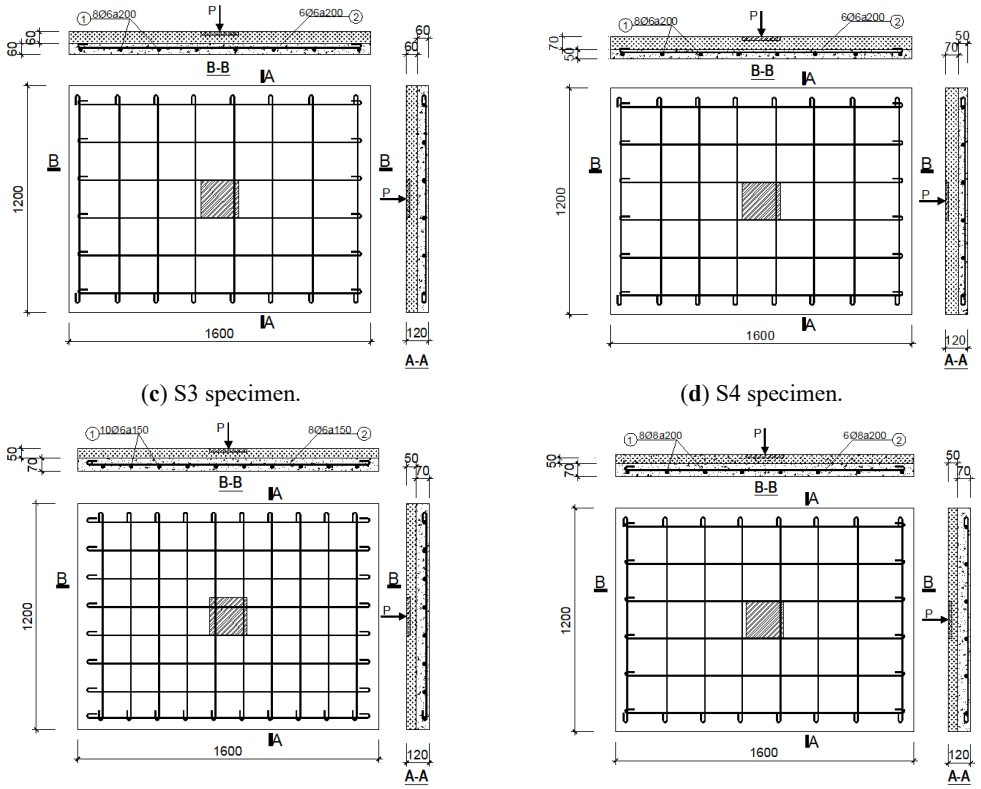

(**c**) S3 specimen. (**d**) S4 specimen.

(**e**) S5 specimen. (**f**) S6 specimen.

Figure 1. Specimen configuration and interface location.

Source: Authors' experimental program.

2.2.2. Material Properties

Two concrete strength grades were used in the experimental program. Grade B15 concrete was used for the monolithic specimen S1 and for the first layer of specimens S2–S6, whereas Grade B20 concrete was used for the second layer of specimens S2–S6. The second layer was cast 14 days after the first layer. The slab tests and the compression tests on the companion concrete specimens were conducted when the second-layer concrete reached an age of 28 days. Consequently, the first-layer concrete was 42 days old at the time of slab testing. The measured compressive strengths at the testing date were 20.7 MPa for the B15 concrete and 25.8 MPa for the B20 concrete. The same sequence of B15 concrete in the first layer and B20 concrete in the second layer was used for all two-layer specimens. However, changing the layer thickness also changed the relative proportions and through-depth distribution of the two concrete grades. Therefore, the S2–S4 comparison represents the coupled effects of interface position and layer-strength distribution rather than the isolated effect of interface position alone.

The reinforcement consisted of plain steel bars with nominal diameters of 6 mm and 8 mm. For the Ø6 bars, the measured yield stress ranged from 280.6 MPa to 284.6 MPa, and the ultimate tensile stress ranged from 484.8 MPa to 488.5 MPa. For the Ø8 bars, the measured yield stress ranged from 280.4 MPa to 284.6 MPa, and the ultimate tensile stress ranged from 481.0 MPa to 487.7 MPa.

These measured properties characterize the concrete and reinforcement used in the specimens. Within each comparison group, concrete grade and steel grade were maintained according to the specimen design and were not treated as independent experimental variables.

2.2.3. Casting Procedure and Interface Preparation

The slab specimens were fabricated using the same general procedure, including reinforcement preparation, formwork installation, concrete casting and curing. Specimen S1 was cast monolithically in one operation over the full thickness of 120 mm. For specimens S2 to S6, the first concrete layer was cast to the target thickness specified in **Table 1**. The second concrete layer was then cast 14 days after the

first layer.

Before the second layer was placed, cement slurry was brushed onto the hardened first-layer surface. The same procedure was used for all two-layer specimens, so differences among S2–S6 were not attributed to different surface preparation. In this test series, the cement slurry represented a practical interface treatment rather than a mechanically roughened or keyed joint.

No mechanical connector, shear key or reinforcement was installed across the horizontal interface. The measured local relative displacement was therefore associated with the initial bond provided by the treated surface, friction after cracking, local restraint, and the global stiffness of the reinforced slab. This detail is important because the reinforcement studied here was ordinary flexural reinforcement; it was not shear-friction reinforcement crossing the interface.

The casting procedure and completed slab specimens are shown in **Figure 2**.

(**a**) Preparation of formwork and reinforcement. (**b**) Completed slab specimens after concrete casting.

Figure 2. Casting procedure.

Source: Authors' specimen preparation.

2.2.4. Test Setup and Instrumentation

The slab specimens were supported continuously along all four edges on 50 mm-wide bearing strips. Based on the overall slab dimensions of 1,200 × 1,600 mm, the clear spans between the inner edges of the supports were 1,100 × 1,500 mm, while the distances between the support centrelines were 1,150 × 1,550 mm. A concentrated load was applied at the slab centre using a hydraulic jack mounted on a steel reaction frame. A 150 × 150 mm steel loading plate, corresponding to a contact area of 22,500 mm^2, was placed beneath the jack to distribute the applied load and reduce local bearing damage.

The applied load was controlled using the hydraulic jack and its pressure gauge. The measured hydraulic pressure was converted to load in kilonewtons using the calibration relationship established by the testing laboratory. The jack–pressure gauge system had been inspected and calibrated in accordance with the laboratory's testing regulations before the experimental program.

Vertical deflection was measured at one position at the centre of the slab using a calibrated dial gauge with a resolution of 0.01 mm. This reading was used to describe the global deformation response of each specimen.

For the two-layer specimens, local relative displacement between the first and second concrete layers was measured in the long-span and short-span directions using calibrated dial gauges with a resolution of 0.01 mm. Each gauge assembly was installed across the casting interface, with its fixing and reference points attached to the two different concrete layers. The measurements were taken over a reference gauge length of 300 mm, and the gauge axis was arranged approximately parallel to the interface. The recorded values therefore represented local relative movement between the layers at the instrumented slab edges. In this paper, the term "interface displacement" refers to the local relative displacement recorded by these dial gauges. Because no independent full-field measurement was available, the readings could not completely separate tangential sliding from possible local rotation or interface opening.

Surface deformation was also measured using dial-gauge extensometers with a reference gauge length of 300

mm. Four measurement positions, PDT-1 to PDT-4, were arranged on the upper slab surface, while PDT-5 to PDT-8 were arranged on the lower surface, as shown in **Figure 3**. The measured change in gauge length was converted to strain using $\varepsilon = \Delta L/L_0$, where ΔL is the measured length change and $L_0 = 300$ mm is the reference gauge length. Strain values are reported in per mille (‰). With a dial-gauge resolution of 0.01 mm, the corresponding nominal strain resolution was approximately 0.033‰. The upper- and lower-surface measurements were used to describe local compressive and tensile strain trends at the instrumented positions. The calculated strain represents the average surface strain over the 300 mm reference gauge length. If visible cracking or localized rotation occurred within this length, the calculated value could include their contribution and should not be interpreted as a pointwise material strain.

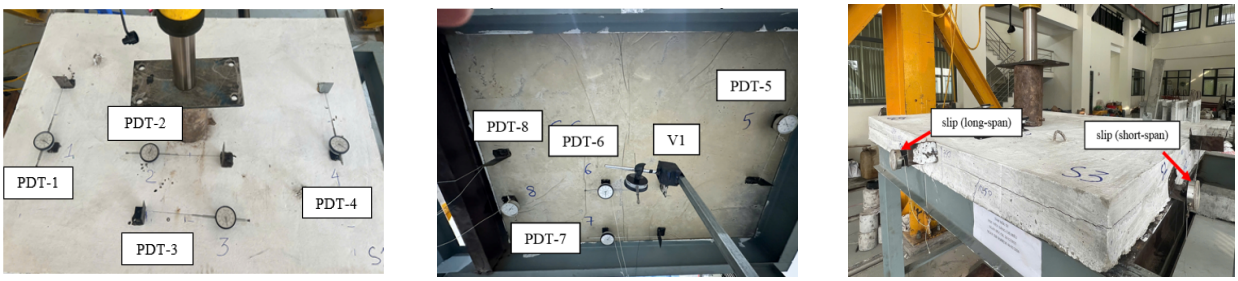

(a) **(b)** **(c)**

Figure 3. Test setup and instrumentation: (**a**) upper-surface deformation measurement positions PDT-1–PDT-4, (**b**) lower-surface deformation measurement positions PDT-5–PDT-8 and central deflection gauge V1, and (**c**) dial-gauge arrangement for measuring local relative displacement between the two concrete layers.

Visible crack initiation and propagation were monitored at successive loading stages, and newly observed cracks were manually marked on the slab surfaces. Crack widths, crack spacing, crack density, and total crack length were not measured quantitatively; therefore, the crack assessment was qualitative. The recorded responses included applied load, central deflection, local interface displacement, surface strain, and visible crack development.

2.2.5. Loading Procedure and Data Processing

The load was applied monotonically through the calibrated hydraulic jack–pressure gauge system. The loading stages were selected from a preliminary estimate of the expected slab resistance and loading procedures adopted in related experimental studies. The adopted loading stages were 0, 6, 13, 19, 25, 31, 38, 44, 50, 56, and 63 kN. At each stage, the load was maintained for approximately 30–60 s to allow the dial-gauge readings to stabilize before the load, central deflection, interface displacement, surface deformation, and visible crack observations were recorded.

Loading was continued until further actuation of the hydraulic jack no longer produced an increase in the recorded load, while the measured displacement continued to increase. The corresponding load was defined as the highest recorded test load, $P_{test,max}$. The recorded values were 50 kN for S1 and S2 and 63 kN for S3–S6. These values represent the highest loads recorded under the adopted test procedure and are not treated as statistically established ultimate capacities. The first visible cracks were identified by direct visual observation and were recorded at the 38 kN loading stage.

The measured data were used to establish load–interface displacement, load–deflection, and load–strain relationships. The load–interface displacement curves were used to compare local relative movement between the concrete layers in the long-span and short-span directions. The load–deflection curves described the global deformation response, while the load–strain curves and visible crack observations were used to interpret the measured post-cracking trends.

The data were interpreted in two stages. First, the monolithic specimen S1 was compared with the reference two-layer specimen S2 to examine the presence of the casting interface. Second, comparisons were made within the two-layer group: S2–S4 for the combined effects of layer arrangement, interface position, and through-depth concrete-strength distribution, and S2–S5–S6 for the combined effects of reinforcement configuration and reinforcement amount. Because each configuration was represented by one specimen, these comparisons describe trends within the tested series rather than statistically verified cause-and-effect relationships.

3. Results

3.1. Load–Interface Displacement Response

The local interface displacement response was examined for specimens S2–S6; no corresponding value was available for the monolithic specimen S1 because it had no casting interface. Measurements were taken in both the long-span and short-span directions because the slabs behaved as two-way members under concentrated loading.

Figures 4 and **5** present the load–interface displacement curves in the two principal directions. In general, the recorded displacement increased with load, although its magnitude and rate of increase differed among the specimens and between the two measurement directions. Relatively small values were recorded before the first visible cracks were observed at the 38 kN loading stage. After visible cracking, several curves showed a more pronounced increase, indicating reduced local compatibility between the concrete layers. Similar interactions between cracking, bending deformation, and concrete-to-concrete interface response have been reported in previous studies [3,10,14].

In the long-span direction, S4 recorded the largest local interface displacement, approximately 6.88 mm at the instrumented edge. This value was substantially greater than the corresponding readings of the other two-layer specimens. Compared with S2, which had the same Ø6@200 mm reinforcement but a 70 + 50 mm layer arrangement, S4 showed a markedly larger long-span value. Within the tested series, the markedly larger displacement recorded for S4 was associated with the combined changes in layer arrangement, interface position, and through-depth concrete-strength distribution. Because the measurement was local, the value should not be interpreted as uniform sliding over the entire interface.

Specimens S2, S3, and S4 formed the layer-arrangement comparison group. They had the same reinforcement arrangement but different first- and second-layer thicknesses. Their long-span readings increased in the order S2, S3, and S4. Because changing the layer thickness also changed the relative proportions of B15 and B20 concrete, the measured trend reflects the combined influence of layer arrangement, interface position, and through-depth concrete-strength distribution. It should not be interpreted as the isolated effect of interface depth or as a statistically verified relationship.

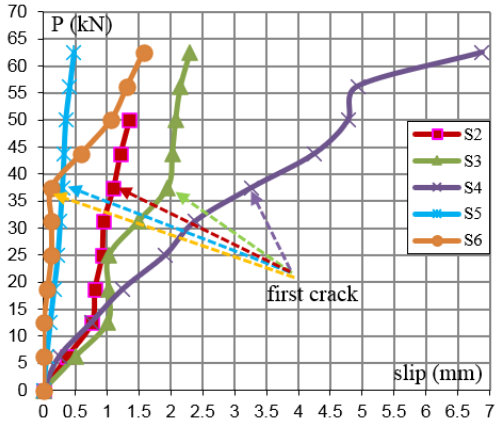

Figure 4. Load–interface displacement curves in the long-span direction.

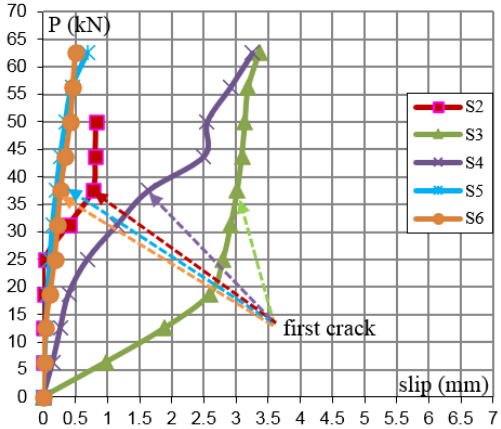

Figure 5. Load–interface displacement curves in the short-span direction.

The short-span curves are shown in **Figure 5**. Although the recorded displacement generally increased with load, the specimen ranking differed from that observed in the long-span direction. This directional difference shows that one measurement direction alone did not represent the complete local interface response of the tested two-way slabs.

In the short-span direction, S3 recorded the largest local interface displacement, approximately 3.36 mm. By comparison, the corresponding values for S2, S5, and S6 were approximately 0.82, 0.69, and 0.50 mm, respectively. Thus, the critical measurement direction differed among the layer-arrangement specimens: S3 was critical in the short-span direction, whereas S4 was critical in the long-span direction. These observations indicate a direction-dependent response within the tested series.

Specimens S2, S5, and S6 had the same 70 + 50 mm layer arrangement but different reinforcement configurations

and reinforcement amounts. Their short-span local interface displacements were approximately 0.82, 0.69, and 0.50 mm, respectively. These values correspond to decreases of about 16% for S5 and 39% for S6 relative to S2 in the short-span direction. However, this comparison does not separate the effects of spacing, bar diameter, and steel area. Moreover, the maximum value for S6 occurred in the long-span direction and reached approximately 1.50 mm, which was greater than the maximum value of 1.30 mm recorded for S2. The apparent benefit was therefore direction-dependent rather than a general reduction in maximum interface displacement.

The highest recorded test load and the local interface displacement did not rank the specimens in the same order. S3–S6 reached 63 kN, but S3 and S4 also recorded the largest directional interface displacements. Consequently, the highest recorded test load alone did not fully describe local compatibility between the concrete layers.

3.2. First Visible Cracking, Maximum Local Interface Displacement, and Highest Recorded Test Load

The first visible cracks were observed at the 38 kN loading stage for all specimens. Because loading was applied in discrete stages, 38 kN is reported as the stage at which cracking was first visually identified rather than as an exact continuously measured cracking load. For the two-layer specimens, local interface displacement generally became more pronounced after this stage.

The highest recorded test load, $P_{test,max}$, was 50 kN for S1 and S2 and 63 kN for S3–S6. At these respective levels, further actuation of the hydraulic jack did not increase the recorded load, while the measured displacement continued to increase. These values describe the termination condition under the adopted test procedure and are not treated as statistically established ultimate capacities, as shown in **Table 2**.

Table 2. First visible cracking stage, highest recorded test load, and maximum local interface displacement.

Specimen	First Visible Crack Stage, kN	$P_{test,max}$ kN	Maximum Local Interface Displacement, mm	Direction of Maximum Value
S1	38	50	-	-
S2	38	50	1.30	long-span
S3	38	63	3.36	short-span
S4	38	63	6.88	long-span
S5	38	63	0.69	short-span
S6	38	63	1.50	long-span

No local interface displacement is reported for S1 because it was cast monolithically. Among the two-layer specimens, S4 recorded the largest overall value, 6.88 mm in the long-span direction, followed by S3 with 3.36 mm in the short-span direction. S6 recorded a short-span value of 0.50 mm but an overall maximum of 1.50 mm in the long-span direction. Therefore, comparisons of interface response must consider both principal directions rather than only the smaller directional value.

The highest recorded test load was 50 kN for both S1 and S2. However, S1 was monolithic, whereas S2 developed measurable local relative displacement at its casting interface. Within this test series, the introduction of the casting interface did not change the highest recorded load relative to S1, but it altered the local deformation response. Similar global load levels should therefore not be interpreted as evidence of identical composite action. Because S1 was cast entirely with B15 concrete whereas S2 contained both B15 and B20 layers, this comparison is descriptive and does not isolate the effect of the casting interface from the difference in concrete-strength distribution.

S2, S3, and S4 had the same reinforcement configuration but different layer arrangements. Their highest recorded test loads were 50, 63, and 63 kN, respectively. These recorded levels indicate different post-cracking responses within the tested series; however, they should not be interpreted as statistically established ultimate strengths. The local interface response also differed: S3 was critical in the short-span direction, while S4 was critical in the long-span direction.

S2, S5, and S6 had the same 70 + 50 mm layer arrangement but different reinforcement configurations and steel areas. Their highest recorded test loads were 50, 63, and 63 kN, respectively. In the short-span direction, the recorded

local interface displacement decreased from 0.82 mm for S2 to 0.69 mm for S5 and 0.50 mm for S6. These trends were associated with the combined changes in spacing, bar diameter, and reinforcement amount and should not be attributed to any single reinforcement parameter. In addition, S6 recorded an overall maximum value of 1.50 mm in the long-span direction; therefore, its response was not uniformly better than that of S2 in both directions.

Before visible cracking, the recorded local interface displacements were generally small, which is consistent with the presence of initial bond and interface contact. After cracking, several specimens showed more pronounced relative movement as flexural stiffness and local compatibility decreased. The available measurements indicate an association between cracking and interface displacement, but they do not quantify the individual contributions of adhesion, friction, rotation, or interface opening.

3.3. Load–Deflection Response

Vertical deflection measured at position V1 was used to describe the global deformation response of the slabs. The first visible cracks were recorded at the 38 kN loading stage; therefore, the load–deflection curves in **Figure 6** are discussed in relation to the stages before and after this observation. The deflection response was interpreted together with the local interface displacement measurements to compare global slab deformation with local compatibility between the concrete layers.

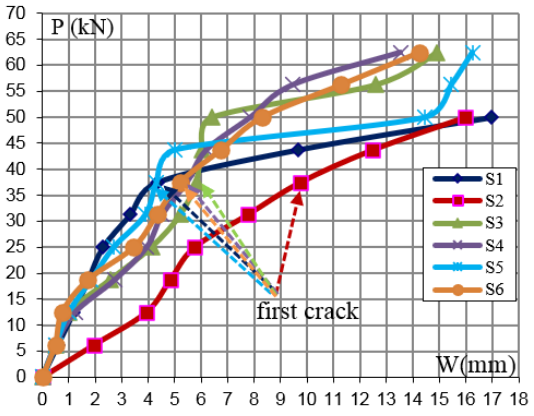

Figure 6. Load–deflection curves of tested slabs.

Source: Authors' experimental results.

Before visible cracking, deflection generally increased with the applied load. At the 38 kN loading stage, the approximate deflections read from **Figure 6** were about 4–5 mm for S1, S4, S5, and S6, whereas S2 recorded a larger value of nearly 10 mm. Within the tested series, S2 therefore showed a less steep pre-cracking load–deflection response than several other specimens. Because one specimen represented each configuration, these differences are reported as observed trends rather than statistically verified stiffness differences.

After the first visible cracks were recorded, several load–deflection curves became less steep, indicating an increase in deformation per unit load. For the two-layer specimens, this change occurred together with increasing local interface displacement. The available measurements therefore indicate an association among visible cracking, global deformation, and reduced local compatibility, although the individual contribution of each mechanism was not quantified.

The highest recorded test load was 50 kN for both S1 and S2. At this load level, the approximate deflection was 16–17 mm for S1 and about 16 mm for S2. Although their recorded load and deflection levels were similar at test termination, their local responses were different: S1 was monolithic, whereas S2 developed measurable relative displacement at the casting interface. This comparison indicates that similar global load–deflection responses do not necessarily represent identical local compatibility.

S2, S3, and S4 had the same Ø6@200 mm reinforcement but different layer arrangements. Their highest recorded test loads were 50, 63, and 63 kN, respectively. At the common load level of 50 kN, the approximate deflection was about 16 mm for S2 and 6–7 mm for S4. Within the tested series, S4 therefore showed a smaller global deflection than S2 at this load level. However, this difference should not be attributed solely to interface position because the layer thicknesses, the through-depth distribution of B15 and B20 concrete, and the local interface responses also differed among the specimens.

S4 illustrates the difference between global and local measurements. At 50 kN, it recorded a smaller vertical deflection than S2, while its maximum local long-span interface displacement reached approximately 6.88 mm. The relatively small global deflection therefore did not correspond to a small local interface reading. Because the dial-gauge measurement was local and could include contributions from sliding, local rotation, or interface opening, the result is inter-

preted as localized loss of compatibility rather than uniform displacement over the entire interface.

The highest recorded test load for S3 was 63 kN, and its approximate deflection near test termination was 15 mm. Its largest local interface displacement was 3.36 mm in the short-span direction. Thus, compared with S4, S3 showed a different combination of global deformation and critical displacement direction. These observations further indicate that the layer arrangement was associated with direction-dependent local behavior within the tested series.

S2, S5, and S6 had the same 70 + 50 mm layer arrangement but different reinforcement configurations and reinforcement amounts. Their highest recorded test loads were 50, 63, and 63 kN, respectively. The load–deflection curves of S5 and S6 extended to the 63 kN loading stage, whereas S2 terminated at 50 kN. These differences were associated with the combined changes in reinforcement spacing, bar diameter, and steel area and cannot be attributed independently to any single reinforcement parameter.

Among the specimens reaching 63 kN, S4 recorded the smallest vertical deflection near test termination, but it also showed the largest local long-span interface displacement. S5 and S6 recorded smaller short-span displacement values than S2; however, the overall maximum value of S6 occurred in the long-span direction and reached 1.50 mm. Therefore, no specimen can be identified as having the most favorable overall response from a single deflection or directional interface-displacement value.

The observed load–deflection trends are qualitatively consistent with previous studies showing that cracking and bending influence the response of concrete-to-concrete interfaces and composite concrete members [3,6,10,18,19]. In the present two-way slabs, global deflection and local interface displacement developed simultaneously, but their magnitudes did not follow the same specimen ranking. This difference supports the combined use of global and local measurements when interpreting layered-slab behavior.

3.4. Average Surface-Strain Response

Average surface strain was calculated from the length changes measured by the dial-gauge extensometers over a 300 mm reference gauge length. The representative load–strain curves for the upper-surface measurement positions are presented in **Figure 7**, while those for the lower-surface positions are shown in **Figure 8**. Under the adopted concentrated loading, the upper-surface measurements generally represented compression, whereas the lower-surface measurements generally represented tension. Because deformation was measured only at selected surface positions, the data were not used to reconstruct a complete through-depth strain distribution or neutral-axis position.

Before the first visible cracks were observed at 38 kN, the measured tensile and compressive strains generally increased with load. After this stage, several lower-surface tensile readings increased more rapidly or became more nonlinear, whereas many upper-surface compressive readings changed more gradually. These trends are consistent with the development of flexural cracking in the tensile region and increased deformation after cracking. However, the available gauge arrangement does not permit a quantitative determination of the complete strain profile through the slab thickness.

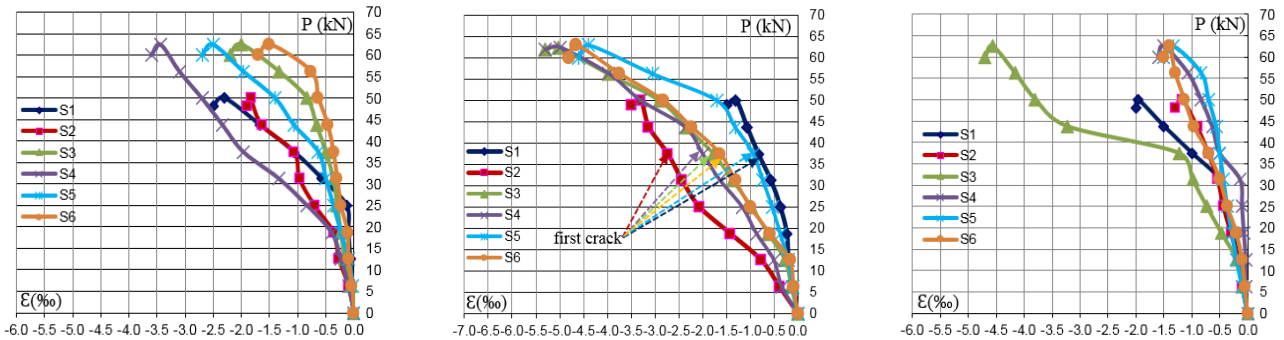

(**a**) PDT-1 and PDT-4 positions. (**b**) PDT-2 position. (**c**) PDT-3 position.

Figure 7. Load–strain responses at the upper-surface measurement positions.

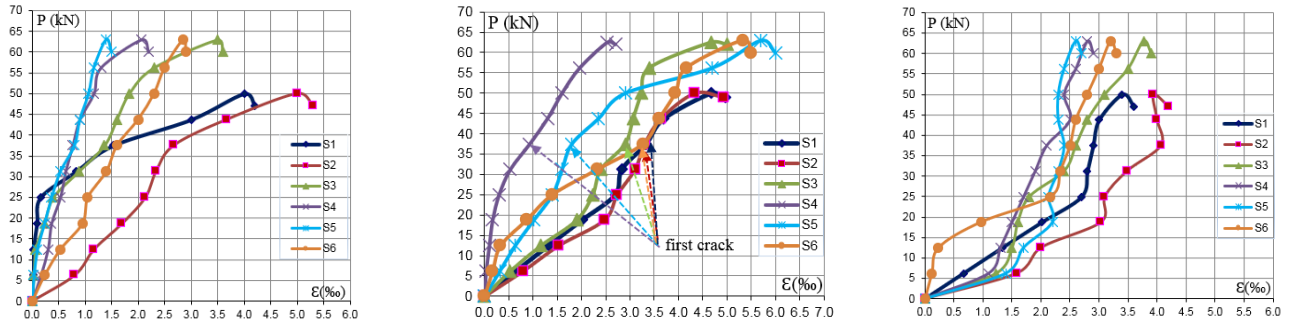

(**a**) PDT-5 and PDT-8 positions. (**b**) PDT-6 position. (**c**) PDT-7 position.

Figure 8. Load–strain responses at the lower-surface measurement positions.

The differences between the upper- and lower-surface strain trends provide complementary information on the slab response. For the two-layer specimens, changes in these trends occurred together with visible cracking and local interface displacement. The measurements are therefore interpreted as qualitative indicators of changing deformation compatibility at the instrumented locations rather than as a complete quantitative measure of composite action.

The highest recorded test load was 50 kN for both S1 and S2. S1 was monolithic, whereas S2 contained a horizontal casting interface and recorded local interface displacement after visible cracking. Differences in their measured strain curves indicate that the local deformation histories were not identical. Nevertheless, because the gauges did not provide a continuous strain profile through the slab depth, the comparison is limited to the recorded instrument locations.

S2, S3, and S4 had the same reinforcement arrangement but different layer thicknesses. Their measured strain curves showed different post-cracking trends, while S3 and S4 also recorded larger directional interface displacements than S2. These observations indicate that the layer-arrangement specimens did not exhibit identical local deformation responses. However, the strain data do not isolate the effects of interface position from those of layer arrangement and through-depth concrete-strength distribution.

For S4, the relatively small vertical deflection was accompanied by the largest local long-span interface displacement. The strain readings at the instrumented positions also differed between the upper and lower surfaces after cracking. Taken together, these measurements are consistent with a distinction between global deformation and localized interface response, although they do not quantify the separate contributions of sliding, opening, or rotation.

S2, S5, and S6 had the same layer arrangement but different reinforcement configurations and steel areas. Their measured tensile and compressive strain curves showed different post-cracking trends, and S5 and S6 reached the 63 kN loading stage. In the short-span direction, S5 and S6 also recorded smaller local interface displacements than S2. These observations were associated with the combined changes in reinforcement spacing, bar diameter, and reinforcement amount; the experimental program did not isolate the individual influence of each parameter.

In several specimens, the lower-surface tensile readings changed more markedly after visible cracking than the upper-surface compressive readings. This trend is consistent with flexural cracking and increasing tensile-zone deformation. Because crack widths were not measured and the gauges were local, the strain data are used only to describe the recorded tendencies and not to quantify crack opening or full-section strain compatibility.

Previous studies have shown that concrete-to-concrete interfaces subjected to combined bending and shear may exhibit behavior different from that observed in direct-shear specimens[3,10,18,19]. In the present tests, the strain readings, vertical deflection, visible cracking, and local interface displacement changed concurrently after cracking. The strain measurements therefore provide supporting local evidence but do not independently quantify the degree of composite action.

3.5. Crack Development and Test Termination Observations

Visible crack development was monitored at successive loading stages, and newly observed cracks were manually

marked on the slab surfaces. Representative crack patterns at test termination are shown in **Figure 9**. Because crack width, spacing, density, and total crack length were not measured quantitatively, the observations are interpreted qualitatively and considered together with the load–interface displacement, load–deflection, and load–strain responses.

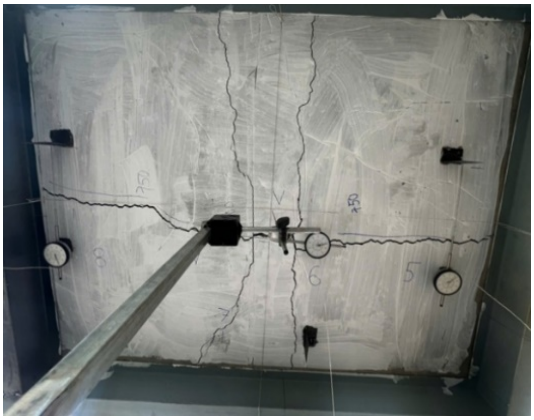

(**a**) S1 specimen.

(**b**) S2 specimen.

(**c**) S3 specimen.

(**d**) S4 specimen.

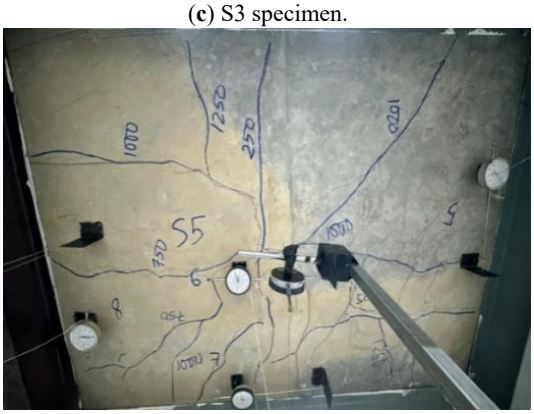

(**e**) S5 specimen.

(**f**) S6 specimen.

Figure 9. Visible crack patterns of the tested slabs at test termination.

The first visible cracks were recorded at the 38 kN loading stage for all specimens. Because the load was applied in discrete stages, this value represents the stage at which cracking was first visually identified rather than an exact continuously measured cracking load. Before this stage, the recorded local interface displacements were generally small.

The monolithic specimen S1 developed visible flexural cracking without a casting interface. Specimen S2 showed a broadly distributed visible crack pattern together with measurable local displacement between its two concrete layers. The highest recorded test load was 50 kN for both specimens; however, their local deformation responses were not identical

because only S2 contained a horizontal casting interface.

The highest recorded test load was 63 kN for both S3 and S4, but the two specimens showed different critical interface-displacement directions. S3 recorded its largest value in the short-span direction, whereas S4 recorded the largest value in the long-span direction. The visible crack patterns provide qualitative evidence of cracking in both principal slab directions, but they do not establish a quantitative relationship between crack width and interface displacement.

Specimens S5 and S6 also reached the 63 kN loading stage. Their short-span interface displacements were smaller than those of S2, but the measurements should be interpreted together with the long-span response. In particular, S6 recorded a maximum long-span value of 1.50 mm, which exceeded the overall maximum value of 1.30 mm recorded for S2. Therefore, the observed response was direction-dependent and cannot be evaluated using only the short-span readings.

At the respective termination levels, further actuation of the hydraulic jack did not increase the recorded load, while displacement continued to increase. The tests therefore ended under a load-plateau condition with continued deformation. Because a complete continuously recorded post-peak response was not obtained, the observed crack patterns and recorded loads are not used to define statistically established ultimate capacities or definitive failure modes.

4. Discussion

4.1. Layer Arrangement and Interface-Location Trends

Specimens S2, S3, and S4 had the same Ø6@200 mm reinforcement and interface treatment but different layer arrangements of 70 + 50 mm, 60 + 60 mm, and 50 + 70 mm, respectively. The first visible cracks were recorded at the 38 kN loading stage for all three specimens. The main differences appeared after visible cracking, particularly in the magnitude and direction of the local interface displacement.

S4 recorded the largest long-span value, approximately 6.88 mm, whereas S3 recorded the largest short-span value, approximately 3.36 mm. S2 showed smaller maximum displacement than both S3 and S4. Within the tested series, these observations indicate that the combined changes in layer arrangement, interface position, and through-depth concrete-strength distribution were associated with direction-dependent local compatibility after cracking. However, because each configuration was represented by one specimen, the results do not establish a statistically verified causal relationship.

The response of S4 illustrates the distinction between global and local behavior. At a common load level of 50 kN, S4 recorded a smaller vertical deflection than S2 but a substantially larger local long-span interface displacement. This result indicates that relatively small global deflection does not necessarily correspond to limited local relative movement between the concrete layers. The local gauge reading may also include contributions from sliding, local rotation, or interface opening and should not be interpreted as uniform displacement over the entire interface.

The observed interaction among bending, cracking, and interface response is qualitatively consistent with studies of concrete-to-concrete interfaces under combined shear and bending and with investigations of composite concrete beams[3,18,19]. However, direct quantitative comparison is limited because the present specimens behaved as two-way slabs and the displacement was measured locally at the slab edges.

Unlike direct-shear specimens, in which relative movement develops mainly along a prescribed loading direction[10,17], the tested slabs developed two-way bending and different critical displacement directions. The present response is closer to the combined bending–shear behavior reported by Cavaco and Camara[3], although the two-way slab geometry introduced additional multidirectional load distribution.

4.2. Reinforcement Configuration and Reinforcement Amount

Specimens S2, S5, and S6 had the same 70 + 50 mm layer arrangement and interface treatment but different reinforcement configurations. The reinforcement areas were approximately 141 mm^2/m for S2, 188 mm^2/m for S5, and 251 mm^2/m for S6. Consequently, the comparison includes simultaneous changes in spacing, bar diameter, and reinforcement amount.

The short-span local interface displacement decreased from approximately 0.82 mm for S2 to 0.69 mm for S5 and 0.50 mm for S6. These values correspond to decreases of

approximately 16% and 39% relative to S2 in the short-span direction. Nevertheless, the overall maximum value for S6 was 1.50 mm in the long-span direction, which was greater than the maximum value of 1.30 mm recorded for S2. The apparent improvement was therefore limited to the short-span measurement and did not represent a general reduction in maximum interface displacement.

S5 and S6 reached the 63 kN loading stage, whereas S2 reached 50 kN. These recorded differences were associated with the combined reinforcement changes but cannot be attributed independently to reduced bar spacing or increased bar diameter. Equal-reinforcement-ratio specimens would be required to isolate these effects.

The reinforcement did not cross the horizontal interface and therefore did not function as conventional shear-friction reinforcement or direct mechanical connectors. Any association between the reinforcement configuration and interface response may have arisen indirectly through changes in flexural stiffness, cracking, and global deformation. Because crack widths and crack spacing were not measured quantitatively, the present results cannot verify the extent to which either configuration controlled crack opening.

The reinforcement-related trends observed in the present slabs differ from those reported for shear-friction reinforcement crossing an interface[6,7,10,11]. In those studies, reinforcement provided direct clamping across the shear plane. In the present specimens, the bars did not cross the interface; therefore, any association with interface displacement may have arisen indirectly through changes in flexural stiffness, cracking, and global deformation.

4.3. Implications for Assessment and Design

The experimental results show that the highest recorded test load alone did not fully represent the local compatibility between the two concrete layers. Specimens S3–S6 all reached 63 kN, but their local interface-displacement responses differed substantially in magnitude and critical direction. Similarly, S4 recorded relatively small global deflection while showing the largest local interface reading. Assessment of a two-layer slab should therefore consider global and local responses together.

The first visible cracks were observed at the 38 kN loading stage, after which several specimens showed more pronounced local interface displacement and deformation. For monitoring or experimental assessment of two-way layered slabs, measurements in both principal directions are preferable because the critical direction differed among the tested specimens. A single directional value may not identify the maximum local response.

EN 1992-1-1, ACI 318-19, AASHTO LRFD, and TCVN 5574:2018 provide strength-based provisions for concrete-to-concrete interfaces. These provisions describe mechanisms such as cohesion, friction, normal restraint, and reinforcement contribution but do not directly predict the local displacement measured in this study. No quantitative code verification was performed because interface roughness, normal stress distribution, and other required parameters were not measured.

The present results also do not establish a permissible or unacceptable interface-displacement limit. The measured values should therefore be used only for comparison within the tested series and should not be treated as code-based serviceability thresholds. For practical staged-casting or repair applications, interface preparation, reinforcement detailing, global deformation, visible cracking, and local interface response should be considered together rather than evaluated through one isolated indicator.

4.4. Limitations and Future Work

The findings describe experimental trends within the tested series. Their generalization is limited by the use of one specimen per configuration, local dial-gauge measurements, qualitative crack observations, discrete loading stages, and the absence of quantitative code verification. Future studies should include repeated specimens, full-field displacement and quantitative crack measurements, equal-reinforcement-ratio comparisons, and analytical or numerical validation.

In the S2–S4 series, changing the interface position also changed the relative thicknesses and through-depth distribution of the B15 and B20 concrete layers; therefore, these effects were not fully isolated.

5. Conclusions

This study compared the local interface displacement and global response of one monolithic and five two-layer reinforced concrete slabs under concentrated loading. Within the limitations of the experimental program, the following

conclusions are drawn:

1. The first visible cracks were recorded at the 38 kN loading stage for all specimens. After this stage, several two-layer specimens showed more pronounced local interface displacement and increasing global deformation. The 38 kN value represents the visual observation stage and not an exact continuously measured cracking load.
2. The S2–S4 series showed direction-dependent local responses associated with the combined changes in interface position and layer-strength distribution. S4 recorded the largest long-span local interface displacement of approximately 6.88 mm, whereas S3 recorded the largest short-span value of approximately 3.36 mm. These results support the measurement of both principal directions when evaluating local interface response in two-way slabs.
3. In the S2–S5–S6 comparison, the short-span displacement decreased from approximately 0.82 mm to 0.69 mm and 0.50 mm, respectively. However, S6 recorded an overall maximum of 1.50 mm in the long-span direction, which exceeded the maximum value of 1.30 mm for S2. The reinforcement-related trend was therefore direction-dependent, and the individual effects of spacing, diameter, and steel area could not be separated.
4. The highest recorded test load was 50 kN for S1 and S2 and 63 kN for S3–S6. At these levels, further actuation of the hydraulic jack did not increase the recorded load, while displacement continued to increase. These values are test-termination loads under the adopted procedure and should not be interpreted as statistically established ultimate capacities.
5. Global and local responses did not follow the same specimen ranking. In particular, S4 combined relatively small vertical deflection with the largest local interface reading. The results therefore indicate that global load and deflection alone are insufficient to describe local compatibility between the concrete layers. Local interface displacement, deflection, strain trends, and visible cracking should be interpreted together.

The study objective was achieved within the limits of the experimental program by jointly evaluating local interface displacement and global slab response. The first and third research questions were addressed by identifying direction-dependent local displacement and showing that global load and deflection alone did not represent local interface compatibility. The second research question was answered only partially because reinforcement configuration, reinforcement amount, interface position, layer arrangement, and concrete-strength distribution were not fully isolated. Accordingly, the hypotheses concerning directional response and the need for combined local–global assessment were supported, whereas the reinforcement- and layer-related hypotheses require further verification. The principal contribution of the study is the simultaneous measurement of local interface displacement in two principal directions together with the global response of two-way layered slabs.

Author Contributions

T.Q.K.L. contributed to conceptualization, methodology, supervision, experimental investigation, validation, and writing-review and editing. C.-H.D. contributed to specimen preparation, experimental investigation, data collection, data analysis. Both authors have read and agreed to the published version of the manuscript.

Funding

This research received no external financial funding.

Institutional Review Board Statement

Not applicable. This study did not involve human participants, animal subjects, clinical samples, pathology reports, or personal data. The experimental program was conducted on reinforced concrete slab specimens under laboratory conditions.

Informed Consent Statement

Not applicable.

Data Availability Statement

The datasets generated and analyzed during the current study are available from the corresponding author upon reasonable request.

Acknowledgments

The authors would like to acknowledge Mien Tay Construction University for providing laboratory facilities and technical support during specimen preparation and experimental testing.

Conflicts of Interest

The authors declare no conflict of interest.

AI Use Statement

No AI tools were used for experimental design, data generation, alteration of experimental results, data analysis, interpretation, or generation of scientific conclusions. All AI-assisted text was critically reviewed, revised, and verified by the authors. The authors take full responsibility for the accuracy, integrity, and scientific content of the manuscript.

References

[1] Beushausen, H., Hohlig, B., Talotti, M., 2017. The influence of substrate moisture preparation on bond strength of concrete overlays and the microstructure of the OTZ. Cement and Concrete Research. 92, 84-91. DOI: https://doi.org/10.1016/j.cemconres.2016.11.017

[2] Bentz, D.P., de la Varga, I., Muñoz, J.F., et al., 2018. Influence of substrate moisture state and roughness on interface microstructure and bond strength: Slant shear vs. pull-off testing. Cement and Concrete Composites. 87, 63-72. DOI: https://doi.org/10.1016/j.cemconcomp.2017.12.005

[3] Cavaco, E., Camara, J., 2017. Experimental research on the behavior of concrete-to-concrete interfaces subjected to a combination of shear and bending moment. Engineering Structures. 132, 278-287. DOI: https://doi.org/10.1016/j.engstruct.2016.11.041

[4] Cavaco, E., Pacheco, I., Camara, J., 2018. Detailing of concrete-to-concrete interfaces for improved ductility. Engineering Structures. 156, 210-223. DOI: https://doi.org/10.1016/j.engstruct.2017.10.058

[5] Jiang, H., Fang, Z., Liu, A., et al., 2016. Interface shear behavior between high-strength precast girders and lightweight cast-in-place slabs. Construction and Building Materials. 128, 449-460. DOI: https://doi.org/10.1016/j.conbuildmat.2016.10.088

[6] Fang, Z., Jiang, H., Liu, A., et al., 2018. Horizontal Shear Behaviors of Normal Weight and Lightweight Concrete Composite T-Beams. International Journal of Concrete Structures and Materials. 12, 55. DOI: https://doi.org/10.1186/s40069-018-0274-3

[7] Liu, J., Fang, J.X., Chen, J.J., et al., 2019. Evaluation of Design Provisions for Interface Shear Transfer between Concrete Cast at Different Times. Journal of Bridge Engineering. 24(6), 06019002. DOI: https://doi.org/10.1061/(ASCE)BE.1943-5592.0001393

[8] Davaadorj, O., Calvi, P.M., Stanton, J.F., 2020. Shear Stress Transfer across Concrete-to-concrete Interfaces: Experimental Evidence and Available Strength Models. PCI Journal. 65(4), 87-111. DOI: https://doi.org/10.15554/pcij65.4-04

[9] Zhang, X., Zhang, W., Luo, Y., et al., 2020. Interface Shear Strength between Self-Compacting Concrete and Carbonated Concrete. Journal of Materials in Civil Engineering. 32(6), 04020113. DOI: https://doi.org/10.1061/(ASCE)MT.1943-5533.0003229

[10] Xia, J., Shan, K.Y., Wu, X.H., et al., 2021. Shear-friction behavior of concrete-to-concrete interface under direct shear load. Engineering Structures. 238, 112211. DOI: https://doi.org/10.1016/j.engstruct.2021.112211

[11] Liu, J., Huang, H., Ma, Z.J., et al., 2021. Effect of shear reinforcement corrosion on interface shear transfer between concretes cast at different times. Engineering Structures. 232, 111872. DOI: https://doi.org/10.1016/j.engstruct.2021.111872

[12] Xu, J.G., Chen, S.Z., Xu, W.J., et al., 2021. Concrete-to-concrete interface shear strength prediction based on explainable extreme gradient boosting approach. Construction and Building Materials. 308, 125088. DOI: https://doi.org/10.1016/j.conbuildmat.2021.125088

[13] Al-Fasih, M.Y., Mohamad, M.E., Ibrahim, I.S., et al., 2021. Experimental and numerical evaluations of composite concrete-to-concrete interfacial shear strength under horizontal and normal stresses. PLoS ONE. 16(5), e0252050. DOI: https://doi.org/10.1371/journal.pone.0252050

[14] Du, W., Yang, C., De Backer, H., et al., 2022. Experimental Investigation on Shear Behavior of the Interface between Early-Strength Self-Compacting Shrinkage-Compensating High-Performance Concrete and Ordinary Concrete Substrate. Materials. 15(14), 4939. DOI: https://doi.org/10.3390/ma15144939

[15] Taklas, M., Leblouba, M., Barakat, S., et al., 2022. Concrete-to-concrete shear friction behavior under cyclic loading: experimental investigation. Scientific Reports. 12, 9451. DOI: https://doi.org/10.1038/s41598-022-13530-5

[16] Feng, S., Xiao, H., Liu, R., et al., 2022. The bond properties between ultra-high-performance concrete and normal strength concrete substrate: Bond macro-performance and overlay transition zone microstructure. Cement and Concrete Composites. 128, 104436. DOI: https://doi.org/10.1016/j.cemconcomp.2022.104436

[17] Monserrat-López, A., Nogales, A., de la Fuente, A., 2023. Experimental characterization of concrete-to-concrete interface shear strength design-oriented constitutive parameters. Structures. 55, 1172-1185. DOI: https://doi.org/10.1016/j.istruc.2023.06.075

[18] Rueda-García, L., Senach, J.L.B., Sosa, P.F.M., et al., 2021. Experimental Analysis of the Shear Strength of Composite Concrete Beams without Web Reinforcement. Engineering Structures. 229, 111664. DOI: https://doi.org/10.1016/j.engstruct.2020.111664

[19] Rueda-García, L., Bonet, J.L., Miguel, P., et al., 2023. Experimental Analysis of the Shear Resistance of Precast Concrete T-beams with a Top Cast-in-place Slab. Engineering Structures. 291, 116462. DOI: https://doi.org/10.1016/j.engstruct.2023.116462

[20] Guan, D., Peng, Z., Chen, Z., et al., 2023. Experimental investigation of interfacial shear behavior between Engineered Cementitious Composite and normal concrete. Case Studies in Construction Materials. 19, e02666. DOI: https://doi.org/10.1016/j.csem.2023.e02666

[21] Abo El-Khier, M., Morcous, G., 2023. Friction and Cohesion Interface Shear Factors of Ultra-High-Performance Concrete (UHPC) Cast on Hardened Conventional Concrete. Buildings. 13(5), 1253. DOI: https://doi.org/10.3390/buildings13051253

[22] Bai, M., Ding, T., Zhao, Y., et al., 2024. Shear performance of new-to-old concrete interface based on various surface preparation techniques and roughness. Case Studies in Construction Materials. 21, e03549. DOI: https://doi.org/10.1016/j.csem.2024.e03549

[23] Kocak, S., Korkmaz, K., Boztas, E., 2022. Impact of polymer coating on the flexural strength and deflection characteristics of fiber-reinforced concrete beams. Journal of Building Material Science. 4(2), 26-35. DOI: https://doi.org/10.30564/jbms.v4i2.5304

[24] Mirzabagheri, S., Salem, O., 2024. Numerical study of GFRP-reinforced concrete beams with straight and hooked-end bar lap splices. Journal of Building Material Science. 6(1), 1-16. DOI: https://doi.org/10.30564/jbms.v6i1.6170

[25] Dahake, H.B., Shinde, B.H., 2025. Mechanical performance of fiber-reinforced self-compacting concrete: Comparative analysis and structural implications. Journal of Building Material Science. 7(2), 122-135. DOI: https://doi.org/10.30564/jbms.v7i2.9694

[26] European Committee for Standardization, 2004. EN 1992-1-1:2004 Eurocode 2: Design of Concrete Structures—Part 1-1: General Rules and Rules for Buildings. CEN: Brussels, Belgium.

[27] ACI Committee 318, 2019. Building Code Requirements for Structural Concrete (ACI 318-19) and Commentary (ACI 318R-19). American Concrete Institute: Farmington Hills, MI, USA.

[28] American Association of State Highway and Transportation Officials, 2024. AASHTO LRFD Bridge Design Specifications, 10th ed. AASHTO: Washington, DC, USA.

[29] Ministry of Science and Technology, 2018. TCVN 5574:2018 Design of Concrete and Reinforced Concrete Structures: Hanoi, Vietnam.